Primitive-Equation-Based Low-Order Models with Seasonal Cycle. Part II: Application to Complexity and Nonlinearity of Large-Scale Atmosphere Dynamics

ULRICH ACHATZ

Leibniz-Institut für Atmosphärenphysik an der Universität Rostock, Kuehlungsborn, Germany

J. D. OPSTEEGH

Royal Netherlands Meteorological Institute, De Bilt, Netherlands

(Manuscript received 21 June 2001, in final form 9 July 2002)

ABSTRACT

A recently developed class of semiempirical low-order models is utilized for the reexamination of several aspects of the complexity and nonlinearity of large-scale dynamics in a GCM. Given their low dimensionality, these models are quite realistic, due to the use of the primitive equations, an efficient EOF basis, and an empirical seasonally dependent linear parameterization of the impact of unresolved scales and not explicitely described processes. Fairly different results are obtained with respect to the dependence of short-term predictability or climate simulations on the number of employed degrees of freedom. Models using 500 degrees of freedom are significantly better in short-term predictions than smaller counterparts. Meaningful predictions of the first 500 EOFs are possible for 4–5 days, while the mean anomaly correlation for the leading 30 EOFs stays above 0.6 for up to 9 days. In a 30-EOF model this is only 6 days. A striking feature is found when it comes to simulations of the monthly mean states and transient fluxes: the 30-EOF model is performing just as well as the 500-EOF model. Since similar behavior is also found in the reproduction of the number and shape of the three significant cluster centroids in the January data of the GCM, one can speculate on a characteristic dimension in the range of a few tens for the large-scale part of the climate attractor. A partial failure diagnosed in the predictability of climate change by our statistical–dynamical models indicates that the employed empirical parameterizations might actually be climate dependent. Understanding their dependence on the large-scale flow could be a prerequisite for applicability to climate change studies. In a further analysis no support is found for the classic hypothesis that the observed cluster centroids, indicating multimodality in the climate statistics, can be interpreted as quasi steady states of the GCM's low-frequency dynamics.

1. Introduction

Recently some new progress has been made in the field of low-order atmosphere models by incorporating primitive equation dynamics and seasonality. In a companion paper (Achatz and Opsteegh 2003, henceforth called Part I), a method has been described for the development of corresponding semiempirical reduced models, combining a primitive-equation-based dynamical core for the nonlinear interactions with an empirical, seasonally dependent, linear closure. This parameterization shall describe simultaneously all diabatic and viscous processes, as well as the impact of unresolved scales onto the resolved ones. The model variables are the expansion coefficients of the atmosphere with respect to a set of three-dimensional empirical orthogonal functions (EOFs) encompassing all dynamical fields. If compared to equally dimensioned quasigeostrophic counterparts in Achatz and Branstator (1999, henceforth called AB99), our models exhibit a much enhanced capability to correctly predict the tendencies of the same GCM that had provided the dataset used for the determination of both EOFs and empirical closure (Voss et al. 1998). This success motivated further tests and applications we want to report here.

We have first examined basic properties of our semiempirical models, such as their ability to predict the daily weather in the GCM and simulate its climate, and their applicability to climate change studies. Simultaneously the predictability tests and climate simulations have provided valuable information with respect to the minimal number of degrees of freedom necessary for a correct dynamical description of the atmosphere. This fundamental theoretical problem is tightly linked to that of the dimension of the climate attractor. Quite a few attempts have been made at corresponding estimates by statistical methods (e.g., Fraedrich et al. 1995; Toth 1995; Wang and Shen 1999). However, the statistical

Corresponding author address: Dr. Ulrich Achatz, Institut für Atmosphärenphysik an der Universität Rostock, Schloßstr. 6, 18225, Kuehlungsborn, Germany.
E-mail: achatz@iap-kborn.de

approach may overlook degrees of freedom which, although small in contribution to the variance, might still be indispensable for a faithful simulation of a system. On the other hand, it can also be that, in spite of a rather large overall dimension, small subsystems exist that are so loosely connected to the rest that a good self-consistent description of those subsystems is possible, incorporating the interaction with the remainder in parameterized form only. An example might be a subspace spanned by the large scales. Systematically reducing the dimension of our EOF models and examining their properties could possibly help in detecting such quasi-autonomous subsystems.

Another question we address concerns the origin of weather regimes and the associated multimodality of the atmospheric probability distribution. Charney and DeVore (1979) have put forward the now classic hypothesis, modified later in various degrees, that multimodality reflects the existence of multiple equilibria of the flow equations. Motivated by the increase of detail in our models, while retaining simplicity, we have decided to reexamine this problem. Our results provide interesting additional constraints to be taken into account by any successful theory on the origin of weather regimes.

The article is structured as follows. In section 2 we analyze the ability of our reduced models to simulate the GCM in its present climate state. We first discuss their capability to predict the daily weather in the GCM and to simulate its seasonally dependent climate statistics. Next we examine the existence of multimodality in the GCM and the reduced models, and compare the corresponding regimes. In section 3 the difficult problem of climate change is addressed. Section 4 contains an extensive test of the multiple quasi-stationarity hypothesis for the origin of multimodality. Section 5 summarizes and discusses the results.

2. Comparison between the EOF models and the GCM

a. Short-term predictions of the GCM

A natural question to ask is how well our low-order models can approximate the local structure of the GCM's attractor. Reproduction of the instantaneous tendencies in the GCM indicates that, if initialized on a GCM trajectory, the reduced models can follow it for quite some time. This has been quantified by calculating mean anomaly correlations [MAC(Δt)],

$$\mathrm{MAC}(\Delta t) = \frac{\sum_{i=1}^{I} (\mathbf{a}_{\mathrm{model}} - \mathbf{a}^s, \mathbf{a}_{\mathrm{data}} - \mathbf{a}^s)(t_i + \Delta t)}{\sum_{i=1}^{I} \left[\|(\mathbf{a}_{\mathrm{model}} - \mathbf{a}^s)(t_i + \Delta t)\|^2 \|(\mathbf{a}_{\mathrm{data}} - \mathbf{a}^s)(t_i + \Delta t)\|^2 \right]^{1/2}}, \quad (1)$$

from integrations initialized twice daily for all days of 9 years of GCM data (i.e., $I = 6480$). The seasonally dependent mean state in the GCM data is denoted by $\mathbf{a}^s(t)$. The rest of the notation is as in Part I.

The results are shown in Fig. 1. The upper panel displays the decay of the mean anomaly correlation between trajectories of the 500-EOF model and GCM trajectories, calculated within the subspaces spanned by the leading 30, 200, or 500 EOFs. Obviously, the higher-dimensional subspaces, which encompass more small-scale features with shorter intrinsic timescales, are more difficult to predict. But even within these, predictions of the GCM with correlations exceeding 0.6 can be made for up to 4.5 days. Moreover, the first 30 EOFs can be predicted well for no less than 9 days.

Part I showed that the accuracy in the prediction of GCM tendencies increases with the number of basis patterns. Nonetheless, even for the 30-EOF model the relative tendency error was not higher than 45.6%. Thus it is no surprise that a comparison of the skill of the 30-, 200-, and 500-EOF model in predicting the leading 30 EOFs shows the more complex models to perform better (lower panel of Fig. 1). However, even the 30-EOF model can predict these degrees of freedom meaningfully for up to 6 days.

b. Monthly mean states and transient eddy fluxes

Next we move to leading characteristics of the global structure of the GCM's attractor, that is, the seasonally dependent monthly mean states and transient eddy fluxes. We first discuss the seasonal dependence of first and second moments in the 500-EOF model, determined from 100-yr integrations. As an example we have picked the January and July mean zonal wind and meridional momentum flux by the transients (defined with respect to the monthly mean state) in the uppermost layer. The mean states of the GCM are very well reproduced by the reduced model (Fig. 2). The momentum transport is simulated well, albeit with a somewhat too weak intensity (Fig. 3). The overall seasonal dependence of the first- and second-moment statistics of the 500-EOF model is thus in quite good agreement with that of the GCM.

How does this comparison depend on the number of basic EOFs? AB99 have noted that their models are best

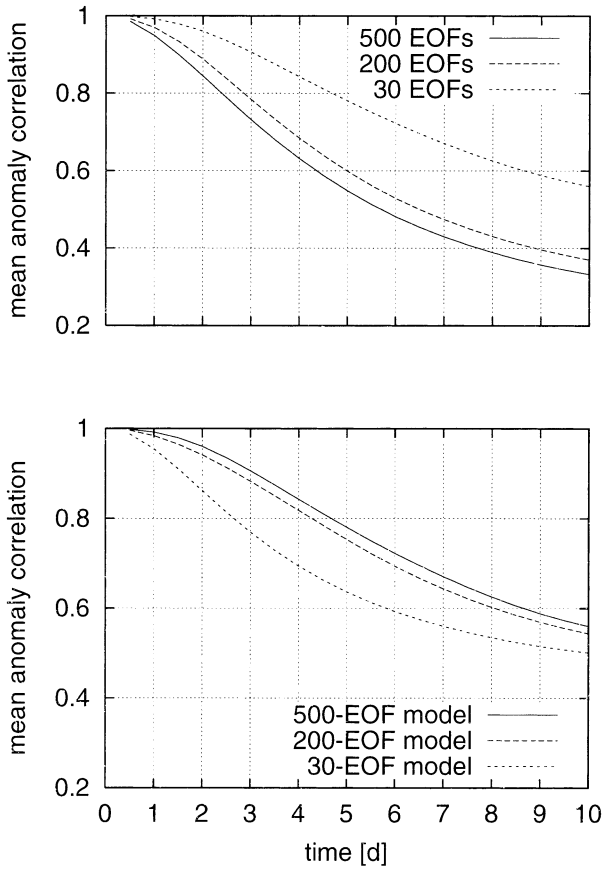

FIG. 1. Mean anomaly correlations between GCM trajectories and those obtained by integration of three semiempirical models. (top) Correlation for the 500-EOF model, calculated in the subspace of the leading 500, 200, and 30 EOFs. (bottom) Correlation in the subspace of the leading 30 EOFs, obtained by integrating the 500-, 200-, or 30-EOF model.

reproducing the first and second moments of the GCM if the chosen resolution was not too fine. An optimum has been found in the range between 30 and 70 basis patterns. This optimum itself might be due to an inability of the quasigeostrophic two-layer model core, used there, to accurately deal with the smaller-scale features represented by the trailing EOFs. However, the interesting aspect of their result is that, as long as the number of basis patterns is larger than 30, the lower-order models are not performing worse than the higher-order ones in reproducing the large-scale aspects of the first- and second-moment structure of the climate attractor, thereby indicating the possible existence of a low-dimensional large-scale subspace connected to the rest so loosely that self-consistent modeling of it is possible to a high degree. The question arises whether we can confirm this finding. In contrast to the models developed by AB99, ours have a seasonal cycle and employ as dynamical core the primitive equations so that an investigation as to what extent this increase in incorporated details has an effect on the resolution dependence of climate simulations, not only with respect to its very existence but also regarding the size of the above mentioned subspace, seemed appropriate. For example, it could have been conceivable that a seasonal cycle requires more than just 30 patterns for a well-performing model.

In agreement with the results of AB99, we find that lower-resolution models are simulating the first- and second-moment statistics of the GCM as well as the 500-EOF model. As objective measures for the comparison between EOF model and GCM data, we have used the relative errors for the monthly mean first and second moments, as defined in Part I. Figure 4 shows once again an optimum at a dimension of 30. Figure 5 shows the corresponding comparison between the transient meridional momentum transport in the uppermost layer in the GCM and in the 30-EOF model. In January the 30-EOF model is clearly in better agreement with the GCM than the 500-EOF model. Further insight is offered by Fig. 6. There, one sees the relative climate error (for a definition see Part I) calculated within different subspaces. In contrast to AB99, we find that within the subspace of the leading 10 or 30 EOFs the 30-EOF model is doing as well as the 500-EOF model, but not better. Obviously, the superiority of the 30-EOF model over the 500-EOF model as displayed in Fig. 4 results from a somewhat worse performance of the 500-EOF model is simulating patterns 31–500. However, once again there is a clear local optimum at a model resolution of 30 EOFs. We conclude that the major result of AB99 is also found for the present semiempirical primitive equation models with seasonal cycle.

c. Recurrent anomalies

Let us now turn to nonlinear signatures in the climate statistics. To some degree it might be sufficient to view nonlinear dynamics as just providing some completely irregular forcing and an effective damping. Assuming maximum irregularity of the forcing in the time domain, that is, stochastic white noise, linear models have been shown to reproduce a wealth of features of the observed climate system (e.g., Farrell and Ioannou 1993, 1994; Penland and Matrosova 1994; Penland and Sardeshmukh 1995; Whitaker and Sardeshmukh 1998; DelSole and Hou 1999; Zhang and Held 1999). However, as is well known (e.g., Honerkamp 1994), the probability density function (PDF) of a stochastically forced linear system is a Gaussian. Therefore, should any deviations from Gaussian statistics be detected, these would indicate the necessity of a more complex model for the active nonlinearity than additive white noise. Indeed, although they are still a matter of debate, indications for persistent and recurrent anomalies have been found by several authors (e.g., Hansen and Sutera 1986; Dole 1986; Molteni et al. 1988, 1990; Mo and Ghil 1988; Michelangeli et al. 1995). These could imply the existence of more than one local maximum of the atmo-

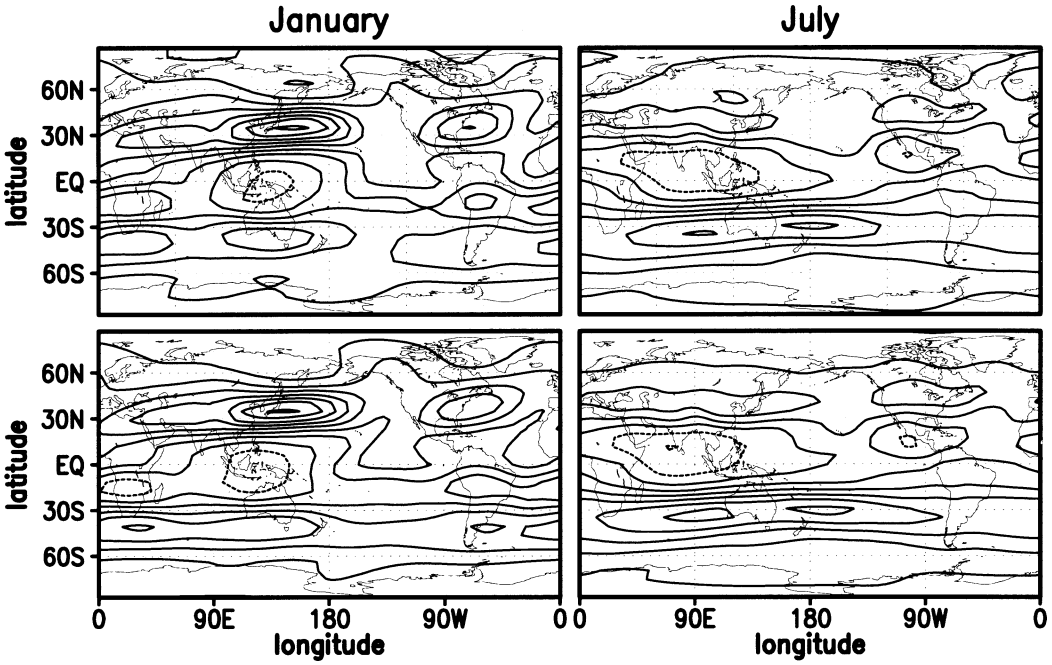

FIG. 2. The Jan and Jul mean zonal wind at $\sigma = 0.167$, as simulated by the (top) semiempirical 500-EOF model and by the (bottom) GCM. Contour intervals are 10 m s^{-1}. Negative contours are dashed.

spheric PDF, an intrinsically non-Gaussian feature. With this in mind we have examined whether the GCM we have used for our work exhibits such features, and, finding this to be true, whether the semiempirical models reproduce them.

For this we have resorted to cluster analysis. The existence of more than one significant cluster in a dataset indicates asymmetries in the corresponding PDF, which might be related to multimodal behavior. We have basically used the method described in Michelangeli et al.

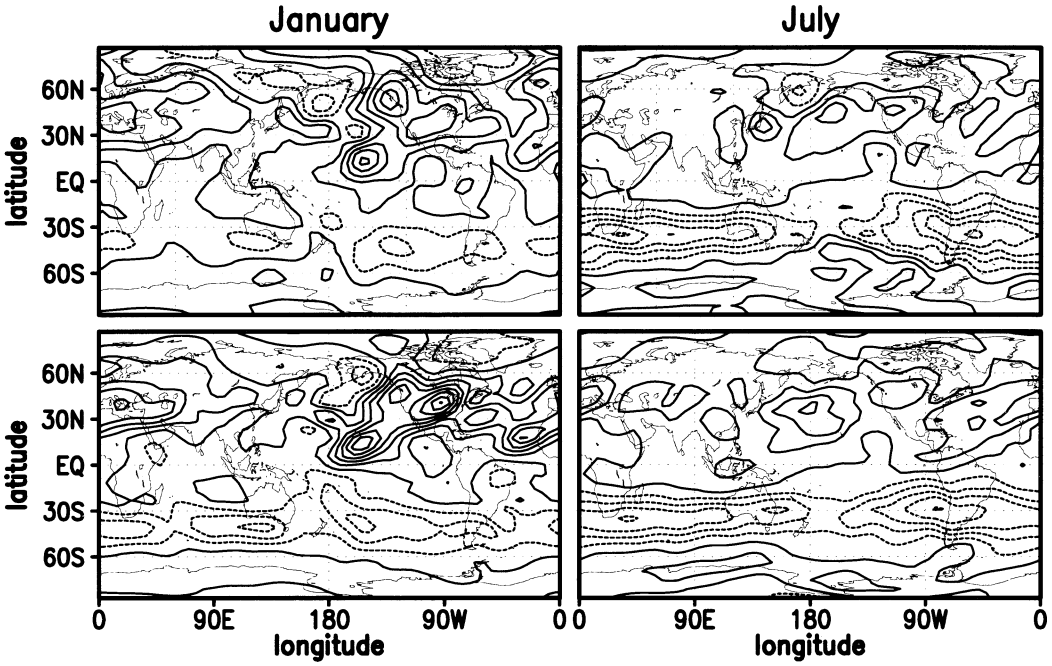

FIG. 3. The Jan and Jul mean meridional momentum transport by the transients (at $\sigma = 0.167$), projected onto the leading 500 EOFs, as simulated by the (top) semiempirical 500-EOF model and by the (bottom) GCM. Contour intervals are 10 m^2 s^{-2}. Negative contours are dashed.

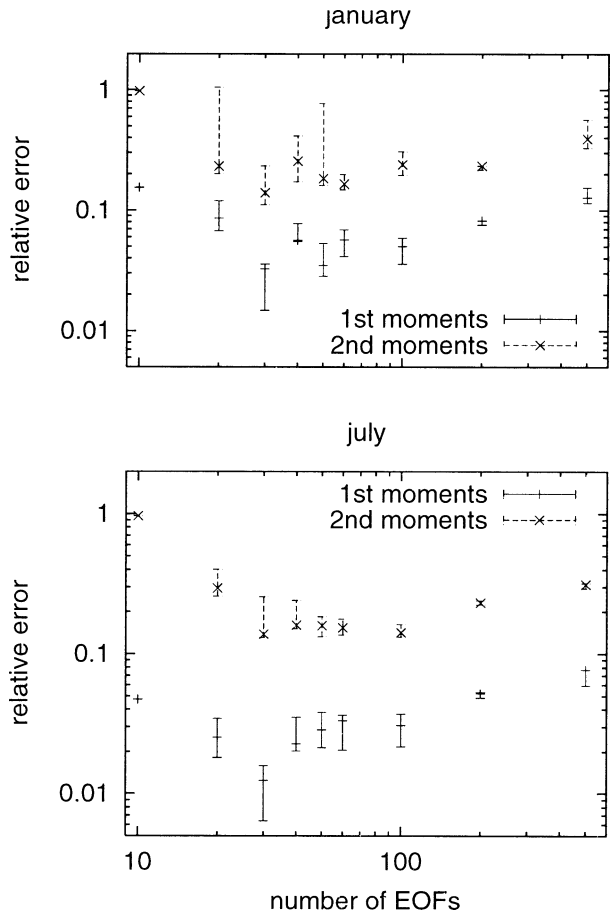

FIG. 4. The relative errors in the simulation of the first and second moments of the GCM by reduced models with different resolution. The errors are computed within the subspace resolved by each model. Shown are the results for Jan and Jul. The error bars (around the errors of the model optimally tuned with respect to the overall climate error) have been obtained by picking the smallest and largest monthly moment error among all cases examined in the optimization of the additional model dissipation (cf. Part I for details) where the mean relative deviation between the optimal dissipation parameter set and the actual parameter set was less than 1%.

(1995), with the modification that, instead of pattern correlations, we have chosen absolute distances between anomalous states as a measure of similarity. Furthermore, we have considered global anomalies involving all prognostic variables. To be more precise, given a dataset of state vectors $\mathbf{b}$, and a predefined number K of centroids $\mathbf{b}_k$ ($k = 1, 2, \ldots, K$), each state is associated with the closest centroid; that is, it is said to belong to the corresponding cluster M_k. The dynamic cluster method (Diday and Simon 1976) determines the centroids such that the sum of variances within the clusters is minimized; that is,

$$\sum_{k=1}^{K} \sum_{\mathbf{b} \in M_k} \|\mathbf{b} - \mathbf{b}_k\|^2 \tag{2}$$

must be as small as possible. Obviously, one will always find a set of cluster centroids minimizing (2). The question is whether they are significant in the sense that they are indicating a clear deviation of the PDF from a Gaussian form. Different initial guesses for the centroids will only result in one final optimal solution if the PDF has a relatively marked multimodal structure. Therefore, choosing a random set of initial guesses, performing the cluster analysis, and finally checking whether the obtained centroids are identical or not, provides a possibility to check the significance of the cluster partitions. As a measure of the uniqueness of the partition in a given number of clusters, that is, the classifiability of the dataset, we have used an index that is defined in the following way. Let P and Q be two partitions of the dataset in K clusters with corresponding cluster centroids $\mathbf{b}_k^P$ and $\mathbf{b}_k^Q$. The difference $d(P, Q)$ between the partitions is given by

$$d(P, Q) = \max_{1 \le i \le K} \min_{1 \le j \le K} \|\mathbf{b}_i^P - \mathbf{b}_j^Q\|^2. \tag{3}$$

It only vanishes when the two partitions are identical. Given a set S_P of M partitions obtained from random initial guesses our classifiability index C is defined via

$$C^{-1} = \frac{1}{M(M+1)} \sum_{P \in S_P} \sum_{Q \in S_P \setminus \{P\}} d(P, Q). \tag{4}$$

The dataset is only then said to be classifiable into K clusters if the classifiability index is significantly larger than the corresponding indices obtained from cluster analyses of random datasets with Gaussian PDF having the same first and second moments.

In our case we have taken as raw data the coefficients belonging to the N leading GCM EOFs from a specific month, either from the GCM integration or from one of the semiempirical models. Then nonoverlapping n-day averages have been formed. These low-pass-filtered states have been analyzed for (low frequency) EOFs, of which the leading $\tilde{N}$ have been picked. The corresponding low-frequency-EOF expansion coefficients of the anomalies with respect to the long time monthly mean form the state vector $\mathbf{b}$. As in Michelangeli et al. (1995), the number of initial guesses for the centroids was $M = 50$. They have been obtained from a random vector generator producing a Gaussian statistics with the same first and second moments as the analyzed data. For comparison 100 random datasets of the same length and with that same Gaussian statistics have been generated, which have then also been analyzed for clusters. The obtained classifiability indices have been ordered with respect to their magnitude and the 10th and 90th of them have then been picked so as to provide an estimate of the confidence limits for classifiability indices obtainable from data with unimodal Gaussian PDF.

In a first attempt we have analyzed 1500 January or July months from the GCM. The leading $N = 30$ EOFs have been picked. Five-day averages have been taken, and no further data compression has been performed; that is, $\tilde{N} = 30$. The resulting classifiability indices are

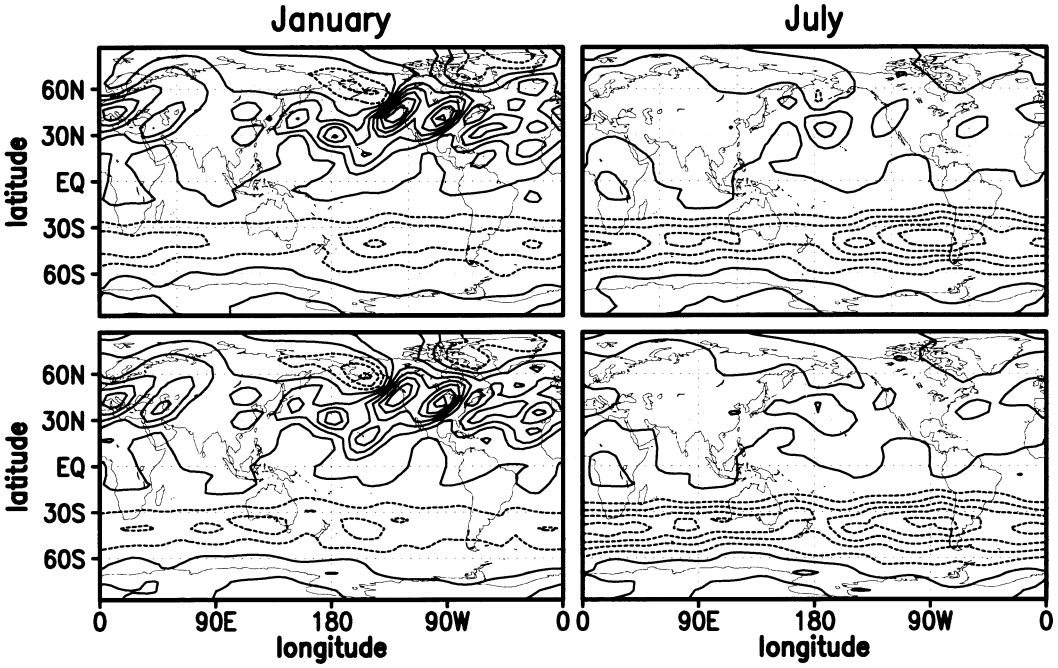

FIG. 5. As in Fig. 3, but for the simulation of the Jan and Jul mean meridional momentum transport by the semiempirical 30-EOF model.

shown in Fig. 7. They indicate that the July PDF can essentially be described by a unimodal Gaussian distribution. However, this is not the case for January. There is a significant classifiability into three clusters. Additionally, we have checked whether we have taken enough data for the analysis by doing a second examination of January months from the first 700 yr. The result was positive: not only was the same behavior of the classifiability index identified, but a comparison of the centroids themselves also showed that they are virtually the same if determined from 700 or 1500 yr.

Henceforth, we have therefore focused our attention on the January PDF, and investigated whether the reduced models can simulate this behavior. The analysis of 1500 January months has been redone with data from the 30-, 200-, and 500-EOF model. Figure 8 contains the classifiability indices determined for the 30-EOF model data. In addition to a weak signal at five clusters, the same significant classifiability into three clusters is discernible. Furthermore, the mean centroids identified for this partition are very similar to the ones obtained from the GCM data. This is displayed in Fig. 9 where the anomalies of the centroids with respect to the mean January state in the barotropic stream functions for both reference partitions (GCM and semiempirical model) are shown. These reference partitions are defined as those among the M determined three-cluster partitions that have, on average, the smallest distance to the other ones. Additional experiments have been done in which the filtering period has been varied between 5 and 30 days, and the compressed dimension $\tilde{N}$ was also changed from 30 to 20, 10, or 5. The results are always about the same. Reproducibility has also been checked by analyzing 3000 instead of 1500 years, with no different outcome.

Cluster analyses of the 200- and 500-EOF model have also been done, in order to analyze the dependence of our results on the truncation. These revealed that, again, the separation into three clusters is significant, and the first two GCM clusters are reproduced (among these, cluster 1 especially well). However, none of the larger models yields a third cluster resembling that in the GCM.

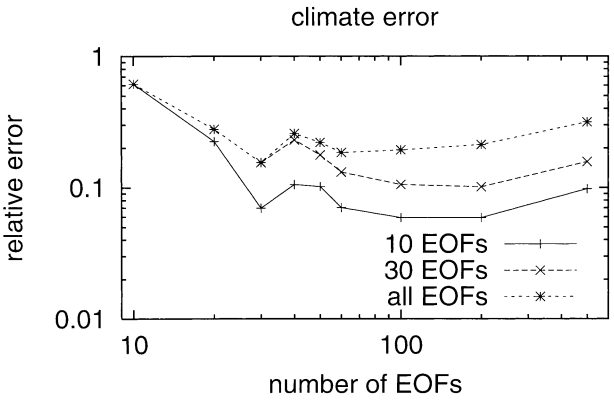

FIG. 6. The climate error of several optimally tuned reduced models, characterizing their performance in simulating the seasonally dependent first and second moments. The calculation has been done in the subspace of the leading 10 EOFs, the leading 30 EOFs, and all EOFs on which the respective model is based.

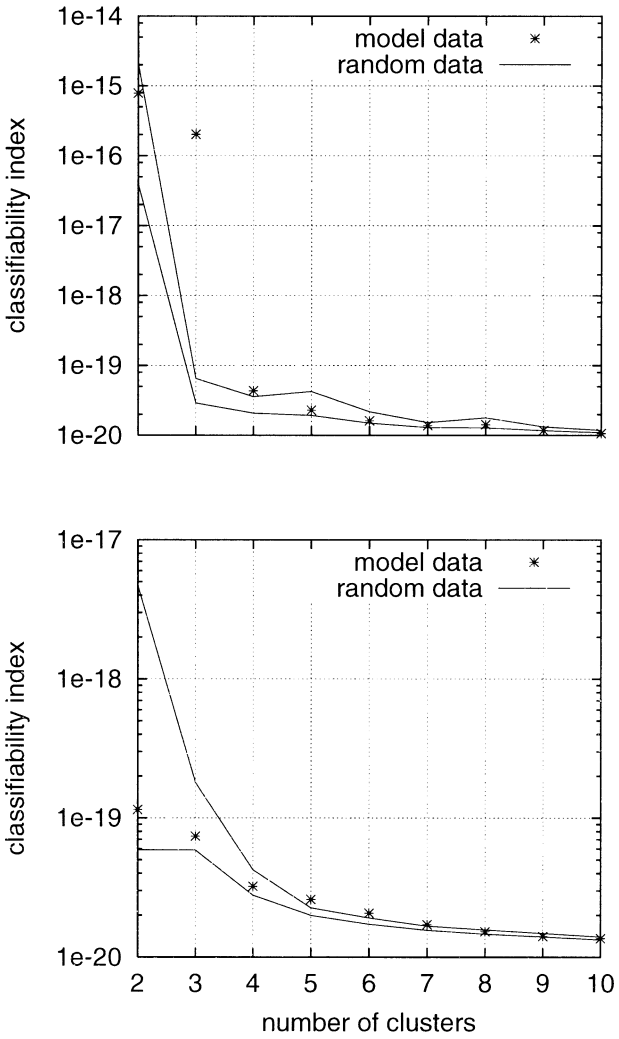

FIG. 7. Classifiability of the GCM data, low-pass filtered by averaging over 5 days, depending on the number of clusters determined in a cluster analysis. The analyzed subspace consists of the coefficients belonging to the leading 30 GCM EOFs. (top) One thousand five hundred Jan months have been analyzed; (bottom) the same number of Jul months.

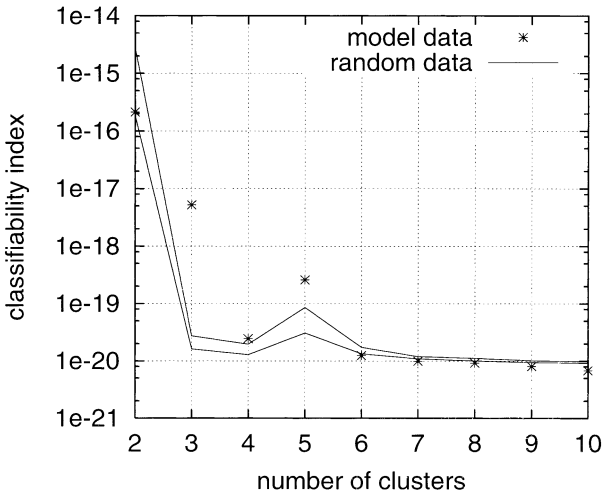

FIG. 8. As in top of Fig. 7, but for the data from the semiempirical 30-EOF model.

3. Response to external perturbations

As pleased as one might be about the ability of our models in simulating the GCM's climate, the important question remains whether they can also be used for studies of climate change or climate variability on ultralong timescales. Problems are to be expected since both optimal patterns and the empirical parameterizations are conditioned on the climate of the dataset from which they have been extracted. For a corresponding investigation we have done some experiments with the GCM in which an anomalous heat source has been placed over the equator. Its form is the same as used by Branstator and Haupt (1998). As a reference the GCM has first been integrated under perpetual January conditions (without coupling to the ocean) and an anomalous response has been determined by subtracting the resulting mean states from the corresponding means from an integration without anomalous heating. The experiment was then repeated with the semiempirical 500-EOF model, followed by a comparison between the responses of the two models.

In a first attempt the reduced model did not respond to the anomalous heating. Inspection showed this to be a consequence of the weak variability of tropical temperature. Corresponding anomalies are rather represented by the trailing EOFs so that anomalous tropical heat sources do not project well onto the leading patterns. We have therefore repeated the original EOF analysis (as described in Part 1), this time, however, splitting the total state space into two subspaces: one subspace comprising the thermodynamic variable τ (the square root of potential temperature) in the latitude band from 11.25°S to 11.25°N, and the other subspace comprising the remaining prognostic variables of the dynamical core. It is easily checked that these two subspaces are orthogonal so that an EOF analysis within them yields two sets of basis patterns with the same property. It was found that 200 tropical-τ EOFs are needed to explain 90% of the the variance orthogonal to the two leading (seasonal cycle) patterns. In the other subspace the corresponding number is 500. It has then been examined how well the anomalous heating projects onto the overall 200 + 500 EOFs. The result was encouraging: among the 24 heat sources we have examined (longitude at 0°, 15°E, . . . , 15°W), none was found that projects onto the new basis to less than 80%. We have therefore determined, in the same manner as described in Part I, a semiempirical 700-EOF model from 1510 years of data that was then tested for its response to the anomalous heating.

Three cases have been studied with anomalous heating at 120°E, 150°E, and 180°. The GCM has been

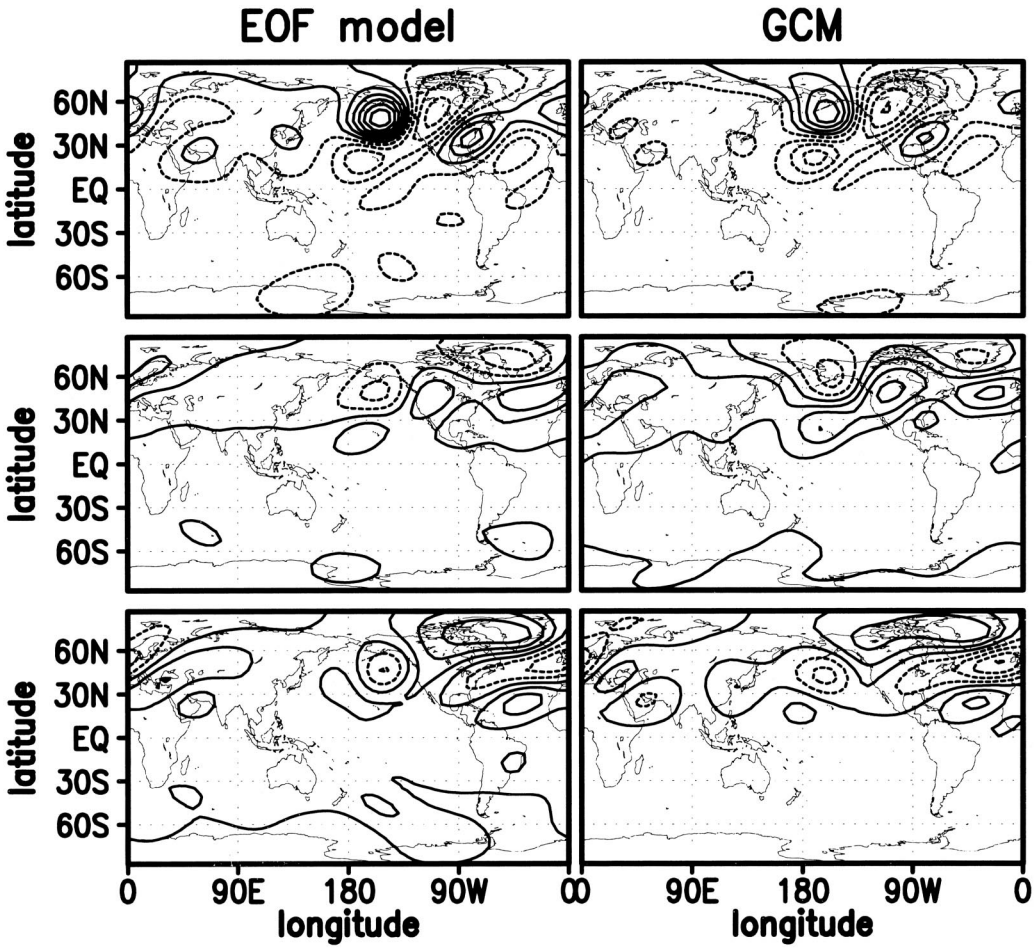

FIG. 9. Barotropic streamfunction anomaly with respect to the Jan mean state in the cluster centroids (top–bottom) 1–3 determined in a three-cluster partition of the time-filtered Jan dataset from the semiempirical 30-EOF model, and from the GCM. Contour intervals are 2×10^{11} Pa m^2 s^{-1}. The percentage of GCM (30-EOF model) states in the clusters is 30% (27%), 40% (38%), and 30% (35%). Negative contours are dashed.

integrated over 36 months, of which the last 30 months have been used for the analysis. The resulting signal-to-noise ratio was sufficient for our needs. The reduced model has been integrated over 5500 days. Here the last 5000 days have been analyzed. The comparison between the two responses was only partially satisfying. Whereas there is some similarity in the responses to heating at 150°E (Fig. 10) and 180°, the reduced model does not reproduce the GCM's response to anomalous heating at 120°E. It was checked whether this is due to an inability of the chosen EOFs to represent the response, but this is not the case. In further experiments, the heat source has been placed at 30°N, so as to exclude the possibility that problems arise from wave train reflection at the subtropical zero-wind line that might be placed differently in the GCM and the reduced model. However, also in these experiments the response of the GCM and the reduced model did not agree well with each other.

4. Recurrent anomalies and quasi stationarity

Finally we address the question of how well, within the framework of the 30-EOF model, the clusters can be explained (in the best of all cases, even be predicted) as stationary states of the atmosphere. This hypothesis goes back to Charney and DeVore (1979) and has later on, with modifications, been taken up by several authors (e.g., Legras and Ghil 1985; Vautard and Legras 1988; Michelangeli et al. 1995; Hannachi 1997). It has been recognized that stationarity is more likely to play a role for the low-frequency part of the dynamics, in the sense that it is only encountered in some time-mean way, with the transients providing possibly important feedbacks.

In a first attempt we have searched for steady states of the semiempirical model itself. This has been done by identifying states $\mathbf{a}_s$, which minimize the squared relative model tendency $\|\dot{\mathbf{a}}(\mathbf{a}_s)\|^2/\overline{\dot{\mathbf{a}}^2}$ so that it is below a certain threshold (the time of the year was held fixed

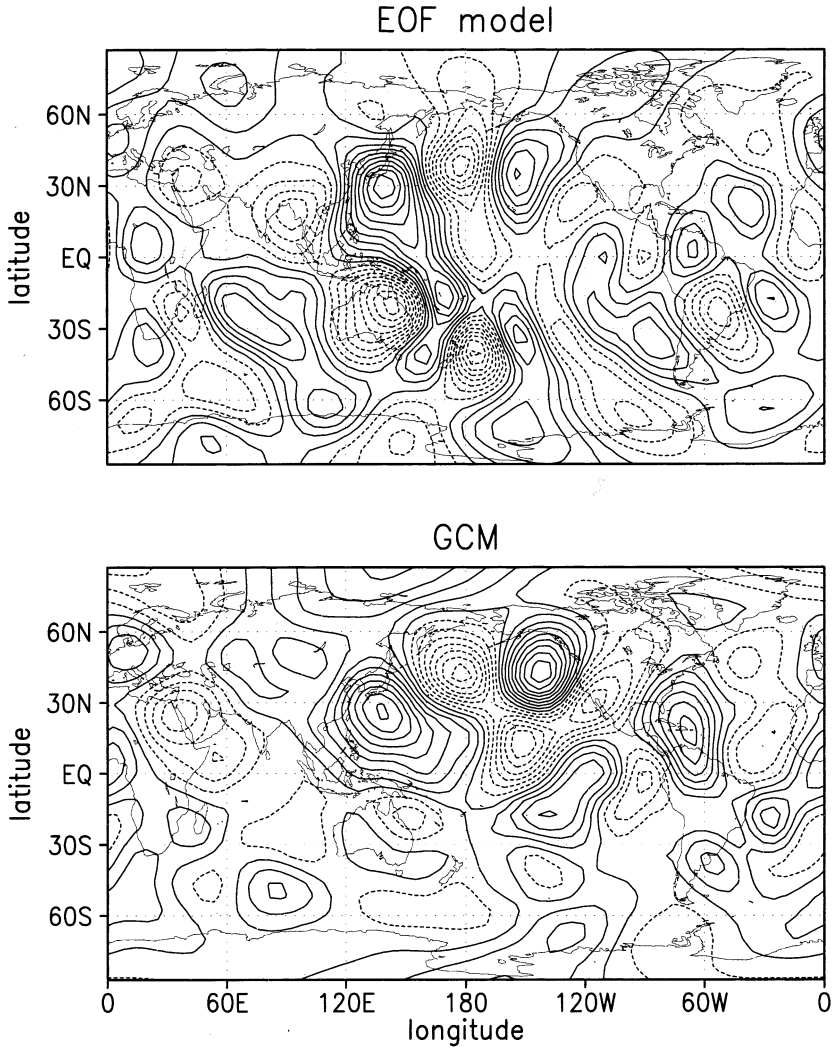

FIG. 10. Response in the meridional wind in the layer at $\sigma = 0.167$ to anomalous heating over the equator at 150°E in the semiempirical EOF model with 200 tropical τ-EOFs and 500 EOFs for global winds, barotropic streamfunction and (top) extratropical τ, and (bottom) in the GCM. Both models have been integrated under perpetual Jan conditions. Contour intervals are 1 m s^{-1}. Negative values are dashed.

at 15 January). For this we used an optimization routine that needs as input a first guess. As such we tried all 9000 January 5-day means that had been used for the cluster analysis. Only solutions with squared relative tendency less than 1.0×10^{-6} have been accepted so that they all represent states that are stationary over periods at least 1000 times longer than the typical timescales produced by the model (a few days). Varying this criterion does not change the outcome greatly. We found 22 steady states. Comparison of these with the three cluster centroids did, however, not yield a single pair with convincing similarity. The same holds for the three local tendency minima we found after initializing the search with the cluster centroids themselves.

Since the cluster partition has been determined from 5-day means, a reason for this discrepancy could have been that the mean impact of transients is not taken into account as an additional force on the time-filtered state. Thus we have formulated a low-frequency reduced model incorporating this effect. The degrees of freedom of this model are summarized in the $\tilde{N}$-dimensional vector **b**, as described in section 2c, of expansion coefficients of the time-filtered data with respect to their EOFs. The dynamical equations have been obtained by the same procedure as used in the determination of our semiempirical models from the GCM data. We have projected the equations of the 30-EOF model onto the low-frequency patterns (i.e., projected the primitive equations onto the patterns) and fitted a constant forcing term and a linear term (without slow seasonal dependence) such that the relative tendency error between data (tendencies

from 5-day averages of exact tendencies from the 30-EOF model) and low-frequency model is as small as possible. The model equations are thus:

$$\dot{b}_\nu = F^p_\nu + \sum_{\mu=1}^{\tilde{N}} L^p_{\nu\mu} b_\mu + \sum_{\mu=1}^{\tilde{N}} \sum_{\rho=1}^{\tilde{N}} N_{\nu\mu\rho} b_\mu b_\rho + F^c_\nu + \sum_{\mu=1}^{\tilde{N}} L^c_{\nu\mu} b_\mu, \quad (5)$$

where $\mathbf{F}^P$, $\mathbf{L}^P$, and $\mathbf{N}$ are determined by the projection, whereas $\mathbf{F}^c$ and $\mathbf{L}^c$ are the closure terms that minimize the relative tendency error. This approach is more comprehensive than the one taken by Hannachi (1997) who has parameterized unresolved scales and processes by a constant forcing.

In order to get some overview, the filtering period in days n and the model dimension $\tilde{N}$ have been varied. Low model dimensions are motivated by the observation that, in the case of 5-day-filtered data, the leading five low-frequency EOFs explain 98% of the cluster centroid anomalies with respect to the January mean. Ninety-five percent are already explained by the leading three EOFs. There seems to be a strong projection of the recurrent anomalies onto the leading EOFs. This is remarkable since, in our time-filtered 30-EOF-model data, no fewer than 20 low-frequency EOFs are needed for explaining 90% of the total variance. The various low-frequency models having been analyzed for steady states, squared relative distances have been calculated in the model state space between cluster centroid anomalies and steady-state anomalies, normalized by the squared norm of the cluster centroid anomalies. For each centroid the closest steady state has been identified. The results are summarized in Table 1. The sobering conclusions one can draw from it is that in no case satisfying closeness between steady state and cluster centroid could be found. There seems to be an advantage in the comparison of steady states of the five-dimensional models with the centroids, which might be due to the strong projection of the latter onto the leading five low-frequency EOFs. On the other hand, the results for three-dimensional models are already worse again so that there is also a lower limit in the dimension appropriate for the analysis, which is higher than the one used by Hannachi (1997). Figure 11 shows the two steady states in the five-dimensional 5-day low-pass model, which are closest to centroids 1 and 3. The strong similarities in the patterns of steady state 3 and centroid 3 (pattern correlation is 0.97) and steady state 1 and centroid 2 (pattern correlation 0.77) are striking but, as in the steady-state analysis of the original 30-EOF semiempirical model, the steady-state anomalies are much stronger than those of the corresponding cluster centroids.

TABLE 1. For the three cluster centroids in the Jan data of the 30-EOF semiempirical model, the steady states of this model and various reduced low-frequency models nearest to each centroid, as well as the total number of steady states N_f found in each model. In the first column fnd$\tilde{N}$ denotes the $\tilde{N}$-dimensional model for n-day low-pass-filtered Jan data of the unfiltered model (which is denoted by f0d30). The number of years used in the analysis is also indicated. For each model the upper row contains the relative squared distance ϵ_i between centroid i and the closest steady state (normalized by the squared distance of the centroid to the January mean), irrespectively whether the latter is also closest to another centroid. The lower row indicates the distance to the ''closest'' steady state so that, in the case of a steady state being closest to several centroids, the steady-state–centroid pair with the smallest relative distance has been picked, and for the remaining centroids, a search among the remaining steady states has been done. Numbers in parentheses denote the index of the steady state (arbitrarily ordered).

Model	N_f	ϵ_1	ϵ_2	ϵ_3
f30d30		1.94 (1)	9.81 (1)	6.17 (1)
(24 000a)	14	1.94 (1)	18.11 (4)	6.19 (2)
f30d5		1.98 (1)	8.53 (1)	1.48 (1)
(6000a)	5	2.23 (4)	11.21 (2)	1.48 (1)
f30d3		0.94 (1)	2.28 (2)	1.71 (2)
(3000a)	3	0.94 (1)	548.54 (3)	1.71 (2)
f5d30		5.50 (2)	9.89 (2)	3.86 (18)
(6000a)	46	5.50 (2)	13.98 (25)	3.86 (18)
f5d5		2.83 (1)	3.05 (1)	1.43 (3)
(6000a)	5	2.83 (1)	12.90 (2)	1.43 (3)
f5d3		5.39 (1)	10.96 (1)	1.02 (1)
(3000a)	3	6.41 (2)	2493.90 (3)	1.02 (1)
f0d30		3.03 (3)	13.38 (4)	7.27 (6)
(1500a)	22	3.03 (3)	13.38 (4)	7.27 (6)

5. Summary and discussion

The properties of the newly developed class of semiempirical low-order (EOF) primitive equation models developed by Achatz and Opsteegh (Part I) have been investigated in extensive comparisons between these models and the GCM they are to simulate. First, focussing on the local structure of the atmospheric attractor, mean anomaly correlations have been calculated between GCM trajectories and those of the various low-order models. Analyzing the 500-EOF model we have found that the GCM trajectories in the state space spanned by all basis patterns can be predicted with meaningful skill for up to 4.5 days. The leading 30 patterns are predicted well for up to 9 days. An investigation of the effect of the model dimension reveals a decline of the short-term predictive properties with a decreasing number of basis patterns. Nonetheless, even a 30-EOF model can predict its degrees of freedom well for up to 6 days.

With regard to simulations of the first- and second-moment climate statistics we find, in agreement with the results of AB99 that a 500-EOF model is simulating the atmosphere's climate (as captured by the GCM) well, now, however, also in its seasonal dependence. This indicates that the seasonal cycle is rearranging the respective role of the various atmospheric degrees of freedom rather than using different ones in different seasons. We have also reproduced the observation of the above-mentioned authors that both first and second moments in the respective model state spaces are simulated just as well by lower-resolution models. The model based

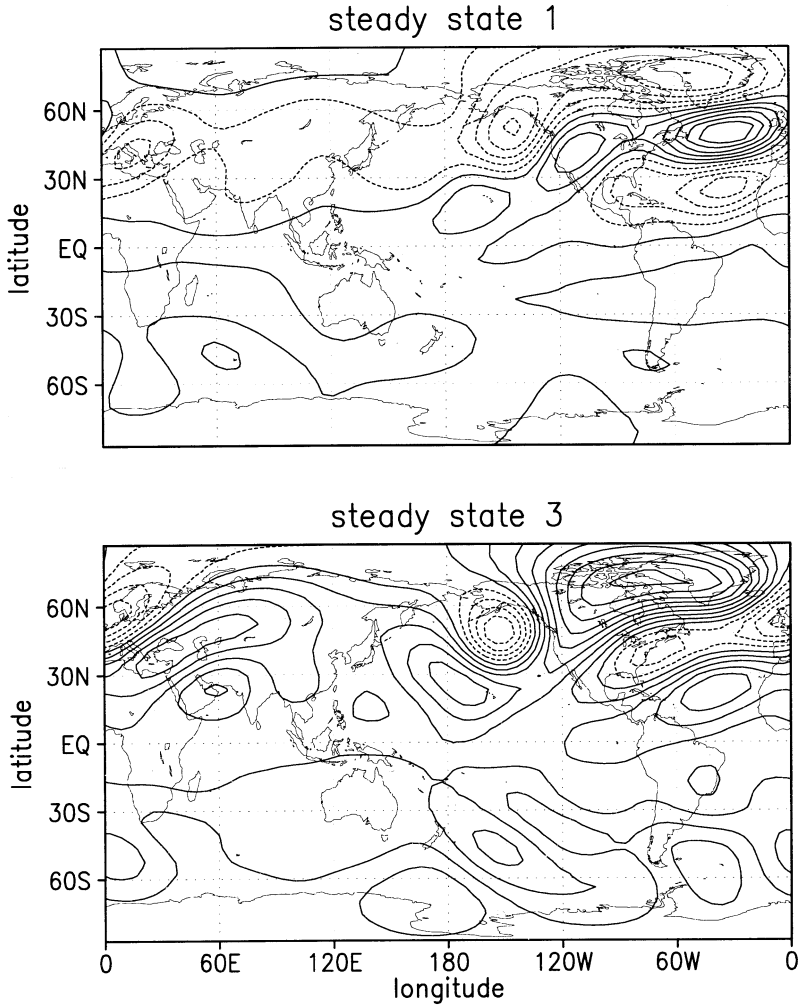

FIG. 11. Barotropic streamfunction anomalies with respect to the Jan mean of the two steady states of the five-dimensional 5-day low-pass low-frequency model closest to cluster centroids 1 and 3 as shown in Fig. 9. Units and contours are the same as there.

on only 30 patterns simulates the seasonally dependent mean states and transient fluxes based on its explicit degrees of freedom faithfully in a selfconsistent manner.

A further feature we have looked at is non-Gaussian statistics. Recurrent anomalies in GCM and reduced models have been searched for by way of a cluster analysis. Care has been taken to detect statistically significant deviations in the PDF from purely Gaussian behavior. We find in the GCM a significant partitioning into three clusters in January. A corresponding analysis of data from the low-order models yields the same result. Here, the 30-EOF model is performing especially well. It reproduces all three recurrent anomalies faithfully as well as the number of states found in their domain.

A caveat must be added concerning the present applicability of semiempirical reduced models in the context of climate prediction. Our work shows that an essential part of the impact of the unresolved scales and physical processes can be described by linear parameterizations. However, the corresponding parameters had to be determined empirically from the GCM data. These are conditioned on the examined climate so that changes in external influences (from radiation, ocean, ice, soil, etc.) should have an effect on them. For the present, we have not undertaken an effort to capture as much of this climate dependence as possible by using explicit physics parameterizations in the dynamical core wherever conceivable, or by trying advanced theoretical approaches such as renormalization group theory (Moise and Temam 2000). This would have reduced the role of the empirical terms to handling only the most intricate feedbacks of the unresolved scales and physics onto the resolved scales, which we are presently not able to parameterize on theoretical grounds. Not too surprisingly, attempts at using our models for predicting the GCM's response to anomalous tropical heating were therefore only partially satisfying. There is still plenty of room for improvements of reduced models, which could fi-

nally make them fully applicable to climate change studies. Even at the present stage, however, it should be stressed that our results do not argue for the use of more basis patterns. Even though a more compact basis might be possible using more dynamically oriented patterns such as principal interaction patterns (Hasselmann 1988; Achatz et al. 1995, Kwasniok 1996, 1997; Achatz and Schmitz 1997) or stochastic optimals (Farrell and Ioannou 2001), at the examined truncation both the anomalous forcing and the true anomalous response are well represented by the chosen EOFs.

It remains a striking observation that a model using no more than 30 basis patterns can simulate many aspects of the GCM's climate as well as its higher-dimensional brothers, and it is tempting to ask for explanations of this behavior. Certainly it must be expected that further improvements in the dynamical model core, for example, increased vertical resolution or explicit treatment of nonlinear physical processes, will finally lead to reduced models that get better as the number of basis patterns is increased. After all, the GCM itself, projected onto a complete EOF basis, would be an EOF model yielding exactly the climate of the GCM data with which we are comparing the reduced models. Nonetheless, there are local optima in model resolution that may still survive further model developments. It might be speculated that the optimum of about 30 EOFs indicates the existence of a typical number characterizing the complexity of that large-scale part of the GCM's dynamics that can be simulated especially well in a selfconsistent manner. Incorporation of only a few additional basis patterns could lead to a worsening of the model performance since they span dynamic components of smaller scale and higher frequency, which can only be well described if all corresponding basis patterns are taken into account. Support for the notion that the local optimum we find at a few tens of basis patterns could be dynamically meaningful comes from previous attempts that have been undertaken at measuring the complexity of the large-scale part of the climate attractor in the form of a number of spatial degrees of freedom (e.g., Lorenz 1969; Livezey and Chen 1983; Horel 1985; Van den Dool and Chervin 1986; Fraedrich et al. 1995; Toth 1995; Wang and Shen 1999). All estimates found the number of degrees of freedom of the atmosphere or GCMs to be in the range of between several tens and slightly above 100. This roughly agrees with the critical number we found where it should be stressed that it is more the optimum at a few tens than the very number 30 we consider important. Further work is necessary to investigate the correctness of this picture but we think it could be a useful working hypothesis.

Since the 30-EOF model is reproducing the clusters of the GCM so well, we have also looked at the question whether the thereby indicated multimodality of the GCM's PDF can be understood by relating the cluster centroids to the steady states of the model. For this, both the reduced model itself has been analyzed and corresponding low-frequency versions. The latter project its dynamics further onto leading low-frequency EOFs, obtained by an analysis of low-pass-filtered data from the 30-EOF model, and utilize in addition an empirically determined parameterization of the impact of transients. The lower dimension of these models (as also used by Hannachi 1997) can be justified by the observation that the cluster centroids project much stronger onto the leading low-frequency patterns than the total variance. The results were not encouraging: none of the models we have looked at, that is, also the 30-EOF model itself, have steady states that are convincingly similar to the cluster centroids. Typically, a large difference in the amplitude of the anomalies was encountered. This is in agreement with the results of others (Michelangeli et al. 1995; Hannachi 1997) so that one might question the usefulness of the concept of quasi stationarity for the interpretation of PDF deviations from unimodal Gaussian behavior. Perhaps there is more perspective in the view of Itoh and Kimoto (1999) that ruins of multiple attractors, to be found at nearby values of some model parameters, lead to the observed multimodal behavior. Anyway, interesting work is ahead of us, and hopefully reduced models will be able to contribute.

Acknowledgments. The authors are indebted to R. Haarsma, F. Kwasniok, G. Schmitz, F. Selten, and A. Timmermann for numerous discussions helping us in different phases of the work. Furthermore we would like to acknowledge the helpful comments of C. Penland, K. Fraedrich, and one anonymous reviewer that led to substantial improvements in the manuscript. Special thanks are due to R. Voss for allowing us to use his GCM data. The enormous help of X. Wang in retreiving those data from the archives is also gratefully acknowledged.

REFERENCES

Achatz, U., and G. Schmitz, 1997: On the closure problem in the reduction of complex atmospheric models by PIPs and EOFs: A comparison for the case of a two-layer model with zonally symmetric forcing. *J. Atmos. Sci.,* **54,** 2452–2474.

——, and G. Branstator, 1999: A two-layer model with empirical linear corrections and reduced order for studies of internal climate variability. *J. Atmos. Sci.,* **56,** 3140–3160.

——, and J. D. Opsteegh, 2003: Primitive-equation-based low-order models with seasonal cycle. Part I: Model construction. *J. Atmos. Sci.,* **60,** 465–477.

——, G. Schmitz, and K.-M. Greisiger, 1995: Principal interaction patterns in baroclinic wave life cycles. *J. Atmos. Sci.,* **52,** 3201–3213.

Branstator, G., and S. E. Haupt, 1998: An empirical model of barotropic atmospheric dynamics and its response to tropical forcing. *J. Climate,* **11,** 2645–2667.

Charney, J., and J. G. DeVore, 1979: Multiple flow equilibria in the atmosphere and blocking. *J. Atmos. Sci.,* **36,** 1205–1216.

DelSole, T., and A. Y. Hou, 1999: Empirical stochastic models for the dominant climate statistics of a general circulation model. *J. Atmos. Sci.,* **56,** 3436–3456.

Diday, E., and J. C. Simon, 1976: Clustering analysis. *Digital Pattern*

Recognition. Vol. 10, *Communication and Cybernetics*, K. S. Fu, Ed., Springer-Verlag, 47–94.

Dole, R. M., 1986: Persistent anomalies of the extratropical Northern Hemisphere wintertime circulation: Structure. *Mon. Wea. Rev.*, **114,** 178–207.

Farrell, B. F., and P. J. Ioannou, 1993: Stochastic dynamics of baroclinic waves. *J. Atmos. Sci.,* **50,** 4044–4057.

——, and ——, 1994: A theory for the statistical equilibrium energy spectrum and heat flux produced by transient baroclinic waves. *J. Atmos. Sci.,* **51,** 2685–2698.

——, and ——, 2001: Accurate low-dimensional approximation of the linear dynamics of fluid flow. *J. Atmos. Sci.,* **58,** 2771–2789.

Fraedrich, K., C. Ziehmann, and F. Sielmann, 1995: Estimates of spatial degrees of freedom. *J. Climate,* **8,** 361–369.

Hannachi, A., 1997: Low-frequency variability in a GCM: Three-dimensional flow regimes and their dynamics. *J. Climate,* **10,** 1357–1379.

Hansen, A. R., and A. Sutera, 1986: On the probability density distribution of planetary-scale atmospheric wave amplitude. *J. Atmos. Sci.,* **43,** 3250–3265.

Hasselmann, K., 1988: PIPs and POPs: The reduction of complex dynamical systems using principal interaction and oscillation patterns. *J. Geophys. Res.,* **93,** 11 015–11 021.

Honerkamp, J., 1994: *Stochastic Dynamical Systems*. VCH Publishers, 535 pp.

Horel, J. D., 1985: Persistence of the 500 mb height field during Northern Hemisphere winter. *Mon. Wea. Rev.,* **113,** 2030–2042.

Itoh, H., and M. Kimoto, 1999: Weather regimes, low-frequency oscillations, and principal patterns of variability: A perspective of extratropical low-frequency variability. *J. Atmos. Sci.,* **56,** 2684–2705.

Kwasniok, F., 1996: The reduction of complex dynamical systems using principal interaction patterns. *Physica D,* **92,** 28–60.

——, 1997: Optimal Galerkin approximations of partial differential equations using principal interaction patterns. *Phys. Rev. E,* **55,** 5365–5375.

Legras, B., and M. Ghil, 1985: Persistent anomalies, blocking and variations in atmospheric predictability. *J. Atmos. Sci.,* **42,** 433–471.

Livezey, R. E., and W. Y. Chen, 1983: Statistical field significance and its determination by Monte Carlo techniques. *Mon. Wea. Rev.,* **111,** 46–59.

Lorenz, E. N., 1969: Atmospheric predictability as revealed by naturally occurring analogues. *J. Atmos. Sci.,* **26,** 636–646.

Michelangeli, P.-A., R. Vautard, and B. Legras, 1995: Weather regimes: Recurrence and quasi stationarity. *J. Atmos. Sci.,* **52,** 1237–1256.

Mo, K. C., and M. Ghil, 1988: Cluster analysis of multiple planetary flow regimes. *J. Geophys. Res.,* **93,** 10 927–10 952.

Moise, I., and R. Temam, 2000: Renormalization group method: Application to Navier–Stokes equation. *Discrete Contin. Dyn. Syst.,* **6,** 191–210.

Molteni, F., S. Sutera, and N. Tronci, 1988: The EOFs of the geopotential eddies at 500 mb in winter and their probability density distributions. *J. Atmos. Sci.,* **45,** 3063–3080.

——, S. Tibaldi, and T. N. Palmer, 1990: Regimes in the wintertime circulation over northern extratropics. I: Observational evidence. *Quart. J. Roy. Meteor. Soc.,* **116,** 31–67.

Penland, C., and L. Matrosova, 1994: A balance condition for stochastic numerical models with application to the El Niño–Southern Oscillation. *J. Climate,* **7,** 1352–1372.

——, and P. D. Sardeshmukh, 1995: The optimal growth of tropical sea surface temperature anomalies. *J. Climate,* **8,** 1999–2024.

Toth, Z., 1995: Degrees of freedom in Northern Hemisphere circulation data. *Tellus,* **47A,** 457–472.

Van den Dool, H. M., and R. M. Chervin, 1986: A comparison of month-to-month persistence of anomalies in a general circulation model and in the earth's atmosphere. *J. Atmos. Sci.,* **43,** 1454–1466.

Vautard, R., and B. Legras, 1988: On the source of midlatitude low-frequency variability. Part II: Nonlinear equilibration of weather regimes. *J. Atmos. Sci.,* **45,** 2845–2867.

Voss, R., R. Saussen, and U. Cubasch, 1998: Periodically synchronously coupled integrations with the atmosphere–ocean general circulation model ECHAM3/LSG. *Climate Dyn.,* **14,** 249–266.

Wang, X., and S. S. Shen, 1999: Estimation of spatial degrees of freedom of a climate field. *J. Climate,* **12,** 1280–1291.

Whitaker, J. S., and P. D. Sardeshmukh, 1998: A linear theory of extratropical synoptic eddy statistics. *J. Atmos. Sci.,* **55,** 237–258.

Zhang, Y., and I. M. Held, 1999: A linear stochastic model of a GCM's midlatitude storm tracks. *J. Atmos. Sci.,* **56,** 3416–3435.